Crowding-induced Organization of Cytoskeletal Elements: II. Dissolution of Spontaneously Formed Filament Bundles by Capping Proteins

Thomas L. Madden and Judith Herzfeld

Department of Chemistry, Brandeis University, Waltham, Massachusetts 02254-9110

Abstract. Through calculations of molecular packing constraints in crowded solutions, we have previously shown that dispersions of filament forming proteins and soluble proteins can be unstable at physiological concentrations, such that tight bundles of filaments are formed spontaneously, in the absence of any accessory binding proteins. Here we consider the modulation of this phenomenon by capping proteins. The theory predicts that, by shortening the average filament length, capping alleviates the packing problem. As a result, the dispersed isotropic solution is stable over an expanded range of compositions.

THE cytoplasm is typically a very crowded solution, containing 20–30 weight % protein (4). It is widely assumed that the behavior of such nonideal solutions is qualitatively similar to that of dilute solutions, with simple quantitative corrections in the form of activity coefficients. There are at least two fundamental problems with this approach. The first is that in crowded solutions asymmetrically shaped particles will spontaneously align due to packing constraints which cause the lateral and longitudinal translational freedom gained upon alignment to exceed the rotational freedom lost (14). Such entropically driven alignment has been observed in solutions of F-actin (2) and in solutions of microtubules (11). Since these "symmetry-breaking" transitions are usually first order, there is usually a range of concentrations for which the single solution is unstable and spontaneously separates into isotropic and anisotropic domains with different compositions. The second problem is the reciprocal nature of the effect of activity coefficients on self-assembly and of self-assembly on activity coefficients.

To take these complexities into account, in an extrapolation from dilute behavior to high concentrations, a statistical thermodynamic treatment is needed that combines the phenomenology of self-assembly observed at lower concentrations with a model of the interactions between particles that become important at higher concentrations. Such an approach has successfully described spontaneous long-range order and osmotic effects in crowded solutions of self-assembling solutes such as sickle-cell hemoglobin (7–9), surfactants (20, 21) and polyaromatic drugs and dyes (12, 17–19). More recently (13), the approach has been extended to consider a solution of two proteins: one that reversibly self-assembles to form filaments and one that does not. Here the most striking feature of the phase behavior is extreme demixing, such that a high-density phase consisting almost exclusively of tightly packed, highly aligned filaments separates from a relatively dilute isotropic phase depleted of the filament-forming protein. This spontaneous filament bundling (i.e., bundling in the absence of "bundling proteins") could not be predicted via the simple use of activity coefficients.

We now wish to consider the effects of filament-binding proteins. In the present paper, we examine the influence of capping proteins on the spontaneous formation of filament bundles under crowded conditions. A capping protein is one which binds reversibly to one end of a filament. In cooperatively formed filaments, filament ends are relatively unstable and the tendency is to form relatively few, long filaments (i.e., few ends). The more numerous the capping molecules and the more strongly they bind, the more they stabilize filament ends and the greater the tendency to form more short filaments (i.e., more ends). The theory thus leads to an estimation of the effects of capping proteins on the filament length distribution and the related changes in spontaneous filament bundling.

The present work is motivated by the importance of capping for control of the aggregation of action (5). Of course, the behavior of actin *in vivo* is complicated by many interactions. Here we consider only reversible self-assembly and capping. The filaments are assumed to be free in solution, with no cross-links or anchors. Thus the predicted behavior represents a baseline or reference scenario upon which other reversible attachments (e.g., by cross-linkers and anchors) elaborate.

Methods

Our system contains two solutes, " A" and "B". Our model filaments are rigid

Address all correspondence to J. Herzfeld, Brandeis University, P.O. Box 9110, Waltham, MA 02254-9110.

spherocylinders formed by linear associations between A monomers and may, or may not, have a B monomer bound at one end. For the present we will consider only the case in which the radii of the two solutes are the same, $a_A = a_B = a$. This model is, of course, only a crude representation of actin and actin end-capping proteins. Actin filaments are double stranded, which leads to a characteristic stoichiometry and cooperativity of microfilament growth. However, we have found in our studies of sickle-cell hemoglobin that the manifestations of long-range order in crowded self-assembling systems generally depend more on the interactions between particles than on the stoichiometry of assembly (Madden, T. L., and J. Herzfeld, manuscript submitted for publication). Actin filaments are also somewhat flexible, but their persistence length is sufficiently long that description as a rigid rod is a reasonable first approximation. The special features of the more realistic system will be more readily calculated and better appreciated once the features of the simpler model system have been characterized.

To simplify the computation, the filaments are distributed among three mutually orthogonal orientations. The discretization of the particle orientation distribution has also been shown to have minimal effect on predictions of long-range order in self-assembling systems (6). The state of this system can thus be described by specifying the number concentration c_{ijn} of particles with orientation i (i = 1, 2, or 3), of type j (j = α, β, or γ), and aggregation number n. Spherocylindrical particles of aggregation number n are assumed to have the same volume as the n spherical monomers from which they are formed. The particles of type j = α consist entirely of solute A. For j = α, n $\geqslant$ 1. If j = β, the particles are B monomers (n = 1). j = γ indicates an aggregate consisting of a B end-cap and one or more A monomers. For j = γ, n $\geqslant$ 2. Note that while there are three particle types, there are only two solutes: A and B.

The free energy for a given state has four contributions: the free energy of association to form aggregates, which drives aggregate growth; the free energy of mixing, which tends to suppress aggregation; the free energy of hard-core interparticle repulsions, which drives alignment; and the free energy resulting from soft, longer range, repulsions, that oppose alignment of particles. Hence, the free energy density (free energy, in units of kT, per unit volume) is given by:

$$f = f_{assoc} + f_{mix} + f_{hc} + f_{soft} \tag{1}$$

The free energy of association is obtained by assigning a free energy of ϕ_AkT to every contact between two monomers of type A and a free energy of ϕ_BkT for a contact between a monomer of type A and a monomer of type B. Thus,

$$f_{assoc} = -\sum_{ijn} c_{ijn} f_{jn} \tag{2a}$$

with

$$f_{jn} = \begin{cases} \phi_A (n-1) & \text{if } j = \alpha \\ 0 & \text{if } j = \beta \\ \phi_A (n-2) + \phi_B & \text{if } j = \gamma \end{cases} \tag{2b}$$

The remaining three free energy terms, for mixing and interparticle interactions, are formulated as in reference 13. The free energy of mixing is a classical term which derives from the entropy of mixing aggregates of various sizes, compositions and orientations taken as distinct species. The free energy due to hard-core repulsions (i.e., excluded volume) corresponds to the loss of configurational entropy due to the prohibition of interpenetration of particles. This crowding term is calculated using scaled particle theory. The soft repulsions are approximated as a step potential of width ζa and height JkT, and their contribution to the free energy is calculated under the assumption that the potential is weak enough that there is no induction of short range order (Bragg-Williams approximation). This assumption will be valid if the pH is close to the isoelectric point or the ionic strength is very high. Although a sum of positive and negative stop potentials could be used to describe a potential of more realistic shape, we have found that such details of the potential do not have important effects on the long-range order of interest here.

The free energy density of Eq. 1 is a functional of the aggregate size and orientation distribution $\{c_{ijn}\}$. If we define χ_A (χ_B) as the difference between the chemical potential of the solute A (B) and the chemical potential of the solvent, then the equilibrium state is that which minimizes

$$\tilde{f}(\{c_{ijn}\}) = f(\{c_{ijn}\}) - \chi_A v_A(\{c_{ijn}\}) - \chi_B v_B(\{c_{ijn}\}) \tag{3}$$

where

$$v_A = b_1 \sum_{in} (c_{i\alpha n}\, n + c_{i\gamma n}\,[n-1]) \tag{4a}$$

and

$$v_B = b_1 \sum_{in} (c_{i\beta n} + c_{i\gamma n}) \tag{4b}$$

are the volume fractions of solutes A and B, and $b_1 = (4/3)\Pi\alpha^3$ is the volume of a monomer. It follows analytically, from the calculus of variations, that the equilibrium distribution function obeys the symmetry relation

$$c_{i\alpha 1}\exp(-\chi_A b_1) = c_{i\beta 1}\exp(-\chi_B b_1) = K \tag{5a}$$

(for all three directions, i, since the spherical monomers must be istrophically oriented) and the exponential length distributions

$$c_{ijn} = \begin{cases} c_{i\alpha 1}(c_{i\alpha 1}\,\Gamma_i \exp\phi_A)^{n-1} & \text{if } j = \alpha \ (n \geqslant 1) \\ c_{i\beta 1} & \text{if } j = \beta \ (n = 1) \\ c_{i\beta 1}\exp(\phi_B - \phi_A)(c_{i\alpha 1}\,\Gamma_i \exp\phi_A)^{n-1} & \text{if } j = \gamma \ (n \geqslant 2) \end{cases} \tag{5b}$$

where $\Gamma_1 = \Gamma_2 = \Gamma_3$ in the isotropic state and $\Gamma_1 > \Gamma_2 = \Gamma_3$ in the anisotropic (nematic) state. The equilibrium state for given values of χ_A and χ_B is then obtained by numerically minimizing $\tilde{f}$ (Eq. 3) with respect to the parameters K, Γ_1, Γ_2, and Γ_3 in Eq. (5). These parameters define the equilibrium state, including the aggregate size and orientation distributions (Eq. 5), the volume fractions, v_A and v_B, of each solute in the solution (Eq. 4), and the osmotic pressure

$$\Pi = \tilde{f} - \sum_{ijn} c_{ijn} \frac{\delta \tilde{f}}{\delta c_{ijn}} \tag{6}$$

For any value of χ_A (χ_B), the value of χ_B (χ_A) at the isotropic-nematic transition (i.e., where the free energies of the isotropic and nematic states are equal) is found by the numerical methods described in reference 13. For these (χ_A,χ_B) pairs, the corresponding values of v_A and v_B in the isotropic and nematic states describe the compositions of the coexisting isotropic and nematic phases.

Results

The behavior of a ternary system is best represented in a Gibbs diagram. This takes the form of an equilateral triangle (as in Figs. 1 and 2) in which each point specifies the volume fractions of all three species. (This can be done in two dimensions because specifying two volume fractions determines the third, since they must all add up to one.) The vertices of the triangle represent pure samples of each of the three species. Here we have solute A, solute B, and solvent (represented by *). With distance along any line from a given vertex, the volume fraction of the corresponding species decreases linearly, going to zero at the opposite leg. Thus, points on the $*-A$ ($*-B$) leg of the triangle represent binary mixtures of solvent and solute A (B), with no solute B (A). More generally, the points on any line parallel to a given leg of the triangle represent mixtures with the same volume fraction of the species represented by the opposite vertex and a particular point on the triangle may be viewed as the intersection of lines parallel to each of the legs of the triangle which define the volume fractions of each of the species in the mixture. (The equilateral triangle has the virtue that these volume fractions automatically sum to 1 as required.) Consider, for example, the point marked by the dot in Fig. 1 a. This point lies on a horizontal line that is positioned 75% of the way from the base to the apex. All points on this line comprise 75 vol % solvent and 25 vol % solute. At the left (*right*) end of the horizontal line, the solute is all A (B). Since the dot is located 90% of the way across from the left leg to the right leg, it represents a mixture in which 90 vol % of the solute is B and 10 vol % is A.

All the calculated properties of the ternary mixture can be illustrated on the ternary triangle. For each point on the triangle, we calculate the equilibrium distribution of particle

types, sizes and orientations $\{c_{ijn}\}$. This is more information than we can use and it is more convenient to think about a few overall properties. For example, we want to know whether the solution is isotropic ("*I*", when $c_{ijn} = c_{2jn} = c_{3jn}$ for all j and n), or anisotropic (nematic, "*N*"), or separated into coexisting isotropic and nematic phases. The ternary triangle is therefore divided into corresponding regions, as in Fig. 2. Across the phase separated region, lines are drawn which show which isotropic solution (represented by the point at the isotropic end of the line) coexists with which anisotropic solution (represented by the point at the anisotropic end of the line). A mixture with a composition represented by a point on one of those lines separates into isotropic and anisotropic solutions with the compositions represented by the points on the ends of the line. In each of the phases (*I* or *N*) we also want some information on the state of aggregation of the solute. A convenient measure used here is the average aggregation number for A which is given by

$$\langle n_A \rangle = \left[\sum_{in} (c_{i\alpha n}\, n + c_{i\gamma n}\,[n-1])\right] / \left[\sum_{in} (c_{i\alpha n} + c_{i\gamma n})\right] \quad (7)$$

The variation of $\langle n_A \rangle$ with composition can be illustrated on the ternary triangle by suitably spaced contour lines that connect points with the same value of $\langle n_A \rangle$. Different textures are used for contour lines and phase boundaries, in order to show both on the same diagrams.

In this paper, we concentrate on the effects of capping and therefore consider variations only in ϕ_B, the strength of the association of a B monomer with an A particle. The results are presented for $\phi_A = 27$, $J = 1.0$, and $\zeta = 0.10$. The effects of varying ϕ_A and J have been considered in reference 13.

Ideal Limit

The primary effect of capping is a modulation of filament lengths by stabilizing the ends. It is instructive therefore, before presentation of results for the full model, to consider the effects of capping under "ideal" conditions, where the interactions between particles are absent, and the only significant contributions to the free energy (Eq. 1) are the free energy of mixing and the free energy of association (Eq. 2). In the absence of interactions between particles, there is no alignment transition and the solution is always isotropic. Fig. 1 *a* shows contours for the average aggregation number for A, where capping is not favorable ($\phi_B << \phi_A$). A similar diagram was also presented in reference 13. Note that the length contours ran parallel to the right leg, signifying that $\langle n_A \rangle$ depends only on the volume fraction of the aggregating solute, A; in this case, solute B and solvent are interchangeable diluents of A. Results for strong capping ($\phi_A = \phi_B$) are presented in Fig. 1 *b*. The $\langle n_A \rangle$ contours are no longer dependent solely on the concentration of A. Instead each contour follows a nearly constant ratio of volume fractions of A to B, (which would be a straight line that runs from the solvent vertex to the bottom axis). We also see, as expected, that the values of $\langle n_A \rangle$ are much smaller for a given solution composition when capping is strong than when it is weak.

Crowding

Fig. 2 *a* shows the results of the full model for the limiting case in which ϕ_B is sufficiently negative that monomers of solute B do not bind to the ends of the polymers. This phase diagram for $\phi_B = -2$ looks exactly like that shown in figure 3b of reference 13, where B is not allowed to bind to the polymer at all (in effect $\phi_B = \infty$). For low total solute volume fractions (near the apex of the triangle) the contours in Fig. 2 *a* agree with the ideal results in Fig. 1 *a*, as we expect. At higher concentrations, the effects of interparticle interactions become apparent. In the absence of solute B (on the left leg of the triangle), the effect of the excluded volume of solute A on itself is to push more monomer into aggregates so that the $\langle n_A \rangle = 10^{2.0}$ contour occurs at a much

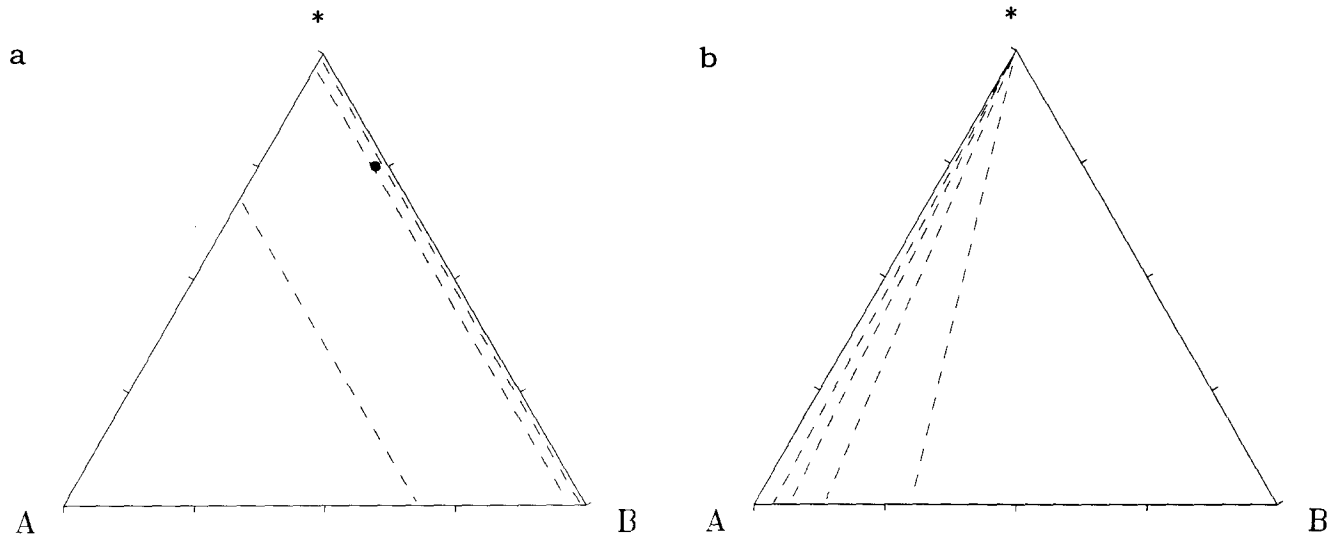

Figure 1. Ternary diagrams with contours for constant average aggregation number $\langle n_A \rangle$ (Eq. 7) for $\phi_A = 27$ in the absence of interparticle interactions. (*a*) $\phi_B = -2$ and the contours from the solvent vertex down are for $\langle n_A \rangle = 10^{1.25}$, $10^{1.5}$, $10^{2.0}$. (*b*) $\phi_B = 27$, and the contours from right to left are for $\langle n_A \rangle = 10^{0.25}$, $10^{0.5}$, $10^{0.75}$, and $10^{1.0}$.

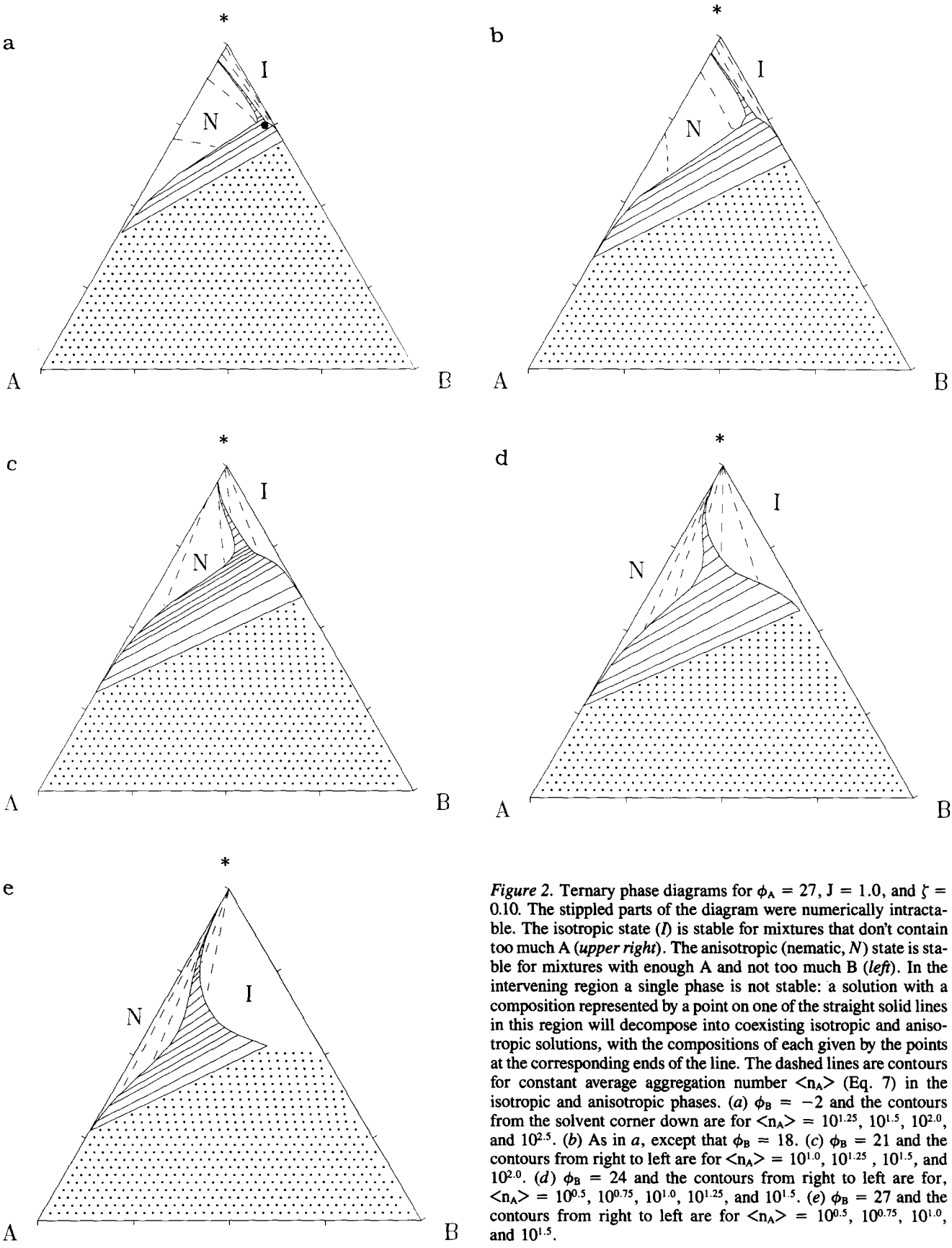

Figure 2. Ternary phase diagrams for $\phi_A = 27$, J = 1.0, and ζ = 0.10. The stippled parts of the diagram were numerically intractable. The isotropic state (*I*) is stable for mixtures that don't contain too much A (*upper right*). The anisotropic (nematic, *N*) state is stable for mixtures with enough A and not too much B (*left*). In the intervening region a single phase is not stable: a solution with a composition represented by a point on one of the straight solid lines in this region will decompose into coexisting isotropic and anisotropic solutions, with the compositions of each given by the points at the corresponding ends of the line. The dashed lines are contours for constant average aggregation number $\langle n_A \rangle$ (Eq. 7) in the isotropic and anisotropic phases. (*a*) $\phi_B = -2$ and the contours from the solvent corner down are for $\langle n_A \rangle = 10^{1.25}$, $10^{1.5}$, $10^{2.0}$, and $10^{2.5}$. (*b*) As in *a*, except that $\phi_B = 18$. (*c*) $\phi_B = 21$ and the contours from right to left are for $\langle n_A \rangle = 10^{1.0}$, $10^{1.25}$, $10^{1.5}$, and $10^{2.0}$. (*d*) $\phi_B = 24$ and the contours from right to left are for, $\langle n_A \rangle = 10^{0.5}$, $10^{0.75}$, $10^{1.0}$, $10^{1.25}$, and $10^{1.5}$. (*e*) $\phi_B = 27$ and the contours from right to left are for $\langle n_A \rangle = 10^{0.5}$, $10^{0.75}$, $10^{1.0}$, and $10^{1.5}$.

lower concentration of A than in the ideal case. Excluded volume interactions also cause the alignment of polymers above ~5 vol % A. The effects of the excluded volume of solute B can be gauged by the effects of replacing solvent by B (i.e., leaving a particular point on the left leg of the triangle along a line parallel to the right leg). Whereas in the ideal case (Fig. 1 *a*), $\langle n_A \rangle$ is unaffected by replacing solvent by B, when interparticle interactions are taken into account (Fig. 2 *a*) we find that $\langle n_A \rangle$ increases as solvent is replaced by B. Again crowding pushes more monomer into polymer. Largely for this reason, the isotropic–nematic transition occurs at lower concentrations of A when B is present.

The most striking feature of this phase diagram is the extreme demixing that eventually occurs as B is added. For example, a mixture of the composition represented by the large dot (~25 vol % protein, of which ~10% is *A*, and ~90% is *B*) will decompose into a dense anisotropic solution of closely packed, highly aligned filaments (~40 vol % protein of which ~88% is *A* and only ~12% is *B*), leaving behind a relatively dilute isotropic solution, somewhat depleted of A and enriched in B. This process is entropically driven. At high concentrations, randomly mixing spherical solutes (*B*) with rodlike solutes (*A*) creates many pockets of wasted space around the spheres and the translational freedom of the rods is reduced in disproportion to the volume actually occupied by the spheres. Demixing relieves this packing problem and yields a gain in translational entropy that exceeds the loss of the entropy of mixing.

Fig. 2 (*b–e*) show the effects of stronger capping (increasing ϕ_B). In all cases, the left legs of the diagrams, where B is absent, are necessarily the same as in Fig. 2 *a*. In Fig. 2 *b* we see that the overall behavior for $\phi_B = 18$ is very similar to that in Fig. 2 *a* where B does not bind. However, at solute volume fractions above 15% there is a noticeable decrease in the average aggregation numbers. This is because crowding drives capping of filaments even though the binding affinity of B is weak. In Fig. 2 (*c–e*) the effects are more dramatic. The average aggregation numbers here depend more on the ratio A/B than on concentration. For a given mixture, the average filament length decreases and the concentration of free B decreases (not shown), as ϕ_B increases. Both of these trends relieve the rod–sphere packing problem. As a result, the region of isotropic stability is progressively expanded and the region of demixing progressively recedes.

Discussion and Conclusions

A typical cell contains about 25 vol % protein, of which perhaps 10% is of a filament forming variety (1, 10, 15). If the other 90% of the protein does not bind to the filaments at all, then the composition of the cytoplasm is represented by the large dot in Fig. 2 *a*. We see that this mixture is unstable and separates into domains with aligned filaments (nematic order) at very high concentrations, coexisting with a more dilute dispersion (isotropic solution) which is depleted of the filament forming solute. Thus we have the spontaneous formation of filament bundles without filament binding proteins. Such crowding-induced bundling has been observed experimentally in mixtures of F-action with nonassociating molecules (3, 16).

Suzuki et al. (16) polymerized G-actin at 0.5 mg/ml in F-buffer containing varying concentrations of the inert polymer poly(ethylene glycol) (PEG)[1], or the soluble protein ovalbumin. These preparations would correspond to points in Fig. 2 *a* on a line parallel to the right leg of the triangle, about 0.05% of the way to the A vertex. Suzuki et al. (16) already find filament bundles when ovalbumin exceeded 15 weight %. This is even stronger demixing than shown in our phase diagrams, which is not surprising considering that the values for the model parameters were not chosen to correspond specifically to the experimental conditions (see below). Both Suzuki et al. (16) and Cuneo et al. (3) have found that PEG induces bundling at a still lower concentration (wt/wt). However these results are difficult to interpret since PEG is not as compact as ovalbumin and its molecular volume will vary with conditions.

In Fig. 2 *a*, the cytoplasmic mixture represented by the dot is close to the isotropic edge of the region of demixing. If some of the nonbinding B were replaced by a capping species B′, then the isotropic solution might be stable and filament bundles might not separate out. This is because the rod–sphere packing problem would be relieved from both directions. When B′ binds to filaments, those "spheres" are removed from the mixture. And, more importantly, by capping filaments, B′ makes the "rods" shorter. To predict the amount of capping protein with a given binding affinity that is required to prevent bundling, it would be necessary to consider the quaternary solvent-A-B-B′ system for which the Gibbs diagram would be a three-dimensional tetrahedron. This is beyond the scope of the present work. However, the series of ternary systems considered here is sufficient to illustrate that the rod–sphere packing problem that drives spontaneous bundling is relieved when otherwise nonaggregating molecules bind to the ends of the filaments. Variations of the quantity and binding affinity of capping proteins are thus two mechanisms by which a cell could control the bundling of reversibly assembled cytoskeletal filaments.

The behavior illustrated here is only for $\phi_A = 27$, $J = 1.0$, $\xi = 0.10$, and $a_A = a_B$. Since ϕ_A, J, and ξ will vary with conditions, there is no one correct set of values. A larger value of ϕ_A would probably be more representative and, by increasing the average filament length, would have the effect of shrinking the isotropic region of the phase diagram and extending the region of extreme phase separation to lower concentrations (i.e., toward the apex of the diagram) (13), as seen experimentally (3, 16). Control of the effective value of ϕ_A, through variations in the concentrations of the effectors of aggregation (e.g., nucleoside triphosphate and calcium), thus represents another mechanism by which the cell may control the formation and dissolution of filament bundles. The region of extreme phase separation is also extended to lower concentrations when the radius of B is less than that of A ($a_B < a_A$) and when soft repulsions are weaker (J is decreased) (13). The reason for not using such parameter values here is that the important qualitative features of the phase behavior are difficult to decipher when compressed into the apex of the phase diagram.

To evaluate the effects of crowding in the highly polydisperse systems of interest, we have made a number of approximations in the theory. However, as discussed in the Methods section, we expect that the results that we have presented here will be qualitatively useful in spite of the sim-

1. *Abbreviation used in this paper*: PEG, poly(ethylene glycol).

plifications used. Our results show that crowding is expected to play an important role in the organization of cytoskeletal elements. Even in the absence of filament binding proteins, packing constraints lead to the spontaneous separation of filament bundles from the cytosol. End capping can dissolve the filament bundles by shifting the filament size distribution to shorter lengths and thereby moderating the difficulty of mixing the variously shaped particles under crowded conditions.

We are grateful to Tom Pollard for his suggestions regarding the presentation of this material.

The work was supported by National Institutes of Health grant HL-36546 and National Research Service Award HL08472 to T. L. Madden.

Received for publication 8 July 1993 and in revised form 1 April 1994.

References

1. Bray, D., and C. Thomas. 1975. The actin content of fibroblasts. *Biochem. J.* 147:221–228.
2. Coppin, C. M., and P. C. Leavis. 1992. Quantitation of liquid-crystalline ordering in F-actin solutions. *Biophys. J.* 63:794–807.
3. Cuneo, P., E. Margri, A. Verzola, and E. Grazi. 1992. "Macromolecular crowding" is a primary factor in the organization of the cytoskeleton. *Biochem. J.* 281:507–512.
4. Darnell, J., H. Lodish, and D. Baltimore. 1986. Molecular Cell Biology. Scientific American Books, New York. 1,192 pp.
5. Hartwig, J. H., and D. J. Kwiatkowski. 1991. Actin-binding proteins. *Curr. Opin. Cell Biol.* 3:87–97.
6. Hentschke, R., and J. Herzfeld. 1989. Nematic behavior of reversibly polymerizing proteins. *J. Chem. Phys.* 90:5094–5101.
7. Hentschke, R., and J. Herzfeld. 1990. Dehydration of protein polymers in concentrated nematic solutions. *Mat. Res. Soc. Proc.* 177:305–310.
8. Hentschke, R., and J. Herzfeld. 1991. Theory of nematic order with aggregate dehydration for reversibly assembling proteins in concentrated solutions: application to sickle-cell hemoglobin polymers. *Phys. Rev. A.* 43: 7019–7030.
9. Herzfeld, J., and M. P. Taylor. 1988. Unexpected critical points in the nematic behavior of a reversibly polymerizing system. *J. Chem. Phys.* 88:2780–2787.
10. Hiller, G., and K. Weber. 1978. Radioimmunoassay for tubulin: a quantitative comparison of the tubulin content of different established tissue culture cells and tissues. *Cell.* 14:795–804.
11. Hitt, A. L., A. R. Cross, and R. C. Williams. 1990. Microtubule solutions display nematic liquid cyrstalline structure. *J. Biol. Chem.* 265:1639–1647.
12. Madden, T. L., and J. Herzfeld. 1992. Exclusion of spherical particles from the neumatic phase of reversibly assembled rod-like particles. *Mat. Res. Soc. Proc.* 248:95–100.
13. Madden, T. L., and J. Herzfeld. 1993. Crowding induced organization of cytoskeletal elements: I. Spontaneous demixing of cytosolic proteins and model filaments to form filament bundles. *Biophys. J.* 65:1147–1154.
14. Onsager, L. 1949. The effects of shape on the interaction of colloidal particles. *Ann. N. Y. Acad. Sci.* 51:627–660.
15. Osborn, M., and K. Weber. 1986. The cytoskeleton. *In* The Organization of Cell Metabolism. G. R. Welch and J. S. Clegg, editors. Plenum Press, New York. 27–36.
16. Suzuki, A., M. Yamazaki, and T. Ito. 1989. Osmoelastic coupling in biological structures: formation of parallel bundles of actin filaments in a crystalline-like structure caused by osmotic stress. *Biochemistry.* 28: 6513–6518.
17. Taylor, M. P. and J. Herzfeld. 1990. A model for nematic and columnar ordering in a self-assembling system. *Langmuir* 6:911–915.
18. Taylor, M. P., and J. Herzfeld. 1990. Phase diagram for reversibly-assembled rod-like aggregates: nematic, columnar, and crystalline ordering. *Mat. Res. Soc. Proc.* 177:135–140.
19. Taylor, M. P., and J. Herzfeld. 1991. Shape anisotropy and ordered phases in reversibly assembling lyotropic systems. *Phys. Rev. A.* 43:1892–1905.
20. Taylor, M. P., A. E. Berger, and J. Herzfeld. 1989. Theory of amphiphillic liquid crystals: multiple phase transitions in a model micellar system. *J. Chem. Phys.* 91:528–538.
21. Taylor, M. P., A. E. Berger, and J. Herzfeld. 1989. A model for nematic phases in a reversibly assembling system of hard rods and plates. *Mat. Res. Soc. Proc.* 134:21–26.